Electrostatic fluctuations in cavities within polar liquids and thermodynamics of polar solvation

Daniel R. Martin and Dmitry V. Matyushov
Center for Biological Physics, Arizona State University, P.O. Box 871604, Tempe, Arizona 85287-1604, USA
(Received 19 June 2008; published 31 October 2008)

We present the results of numerical simulations of the fluctuations of the electrostatic potential and electric field inside cavities created in the fluid of dipolar hard spheres. We found that the thermodynamics of polar solvation changes dramatically when the cavity size becomes about 4–5 times larger than the size of the liquid particle. The range of small cavities can be reasonably understood within the framework of current solvation models. On the contrary, the regime of large cavities is characterized by a significant softening of the cavity interface resulting in a decay of the fluctuation variances with the cavity size much faster than anticipated by both the continuum electrostatics and microscopic theories. For instance, the variance of the electrostatic potential at the cavity center decays with the cavity radius R_0 approximately as $1/R_0^{4-6}$ instead of the $1/R_0$ scaling expected from the standard electrostatics. Our results suggest that cores of nonpolar molecular assemblies in polar liquids lose solvation strength much faster than is traditionally anticipated.

DOI: 10.1103/PhysRevE.78.041206 PACS number(s): 61.20.Ja, 61.25.Em, 82.39.Jn, 77.22.−d

I. INTRODUCTION

Solvation represents the process of inserting a usually molecular-size object into a condensed-phase environment. Since a significant part of chemistry and all life happen in liquid solutions, the traditional focus has been on solvation in liquids, polar liquids in particular. The heterogeneous problem of solvation is probably as complex as the theory of liquids itself and is haunted by the same basic issues making the quantitative description of liquids so challenging. There are two dominating and mutually compensating contributions to the free energy of solvation: The positive free energy of creating a cavity (empty space) for a molecule to be inserted and a negative stabilization energy from short-range (van der Waals) and long-range (electrostatic) forces [1]. The positive free energy of cavity formation is normally significantly compensated by the negative stabilization free energy resulting in the overall solvation free energy often small in comparison with the two components, a situation akin to the competition between repulsive and attractive forces in equilibrium liquids [2].

The present study is devoted to electrostatic solvation, i.e., the free energy arising from electrostatic interactions between the charge distribution of a solute with the charge distribution of a liquid solvent. The charge distribution within molecular solutes is often modeled by atomic partial charges employed by force fields of numerical simulations [3]. On the contrary, the charge distribution of the solvent molecules is often well represented by molecular multipoles following the well established tradition of classical electrostatics [4] and dielectric theory [5]. Extensions to models utilizing atomic charges are also possible as used in numerical simulations [3] and interaction-site models of molecular liquids [2].

Electrostatic solvation is believed to be well understood. Following Born [6] and Onsager [7], the problem is traditionally recast in terms of continuum electrostatics where the electrostatic free energy is sought for the solute charges inserted into a dielectric cavity. This approach has been extensively tested against the experimental database of solvation of small ions and neutral molecules in polar molecular liquids [8]. Despite some inconsistencies, the formalism can be easily incorporated into quantum calculations and can even be quantitative once the dielectric cavity is properly parametrized.

There are however still some fundamental issues that cannot be addressed within electrostatic models. The solution of the Poisson equation in dielectric media is essentially a boundary condition problem in which the assumptions tacitly made by the material Maxwell's equations about the structure of the dielectric interface are essential for the solution. The standard electrostatics assumes abrupt discontinuity of the dipolar polarization at the dielectric surface. This boundary condition creates surface charge [5] which is ultimately responsible for the electrostatic potential within the dielectric cavity. Whether interfaces of real polar liquids [9] match the assumption of abrupt discontinuity of the bulk polarization is an open question. For instance, the electric field within a cavity in a polar liquid was found to be much different from the prediction of standard electrostatics up to the cavity size of a mesoscale dimension [10].

A new additional piece of evidence comes from recent studies of hydrophobic solvation essential for colloid stability, biopolymer folding, and formation of biological supramolecular structures [11,12]. It was found that solvation of nonpolar solutes changes dramatically in character at the length of about 1 nm, which is about three molecular diameters for aqueous solvation [13]. Solvation of solutes larger than this characteristic length was found to be dominated by surface effects, i.e., the structure of water at the hydrophobic interface [13,14]. Weak dewetting [15,16], i.e., a substantial decrease of the water density at the interface compared to the bulk water, was found to be a central part of solvation of large hydrophobic solutes.

Given the current interest in solvation at mesoscale [17,18], to a large extent driven by applications to biology [19–21] and nanoconfinement [22], we address here the problem of electrostatic solvation of solutes significantly larger than have been mostly studied so far. Our study is driven by the question whether the change in the solvation character established for hydrophobic solutes [12] is reflected in an equally dramatic change in the character of electrostatic solvation. The fact that the properties of a polar liquid interface are inconsistent with the assumptions of

Maxwell's electrostatics [10] points to the possibility of a new solution once the size of the solute exceeds some critical dimension. This is indeed the result we report here.

We have found from numerical simulations that the scaling of the fluctuations of the electrostatic potential and electric field with the cavity radius is consistent with the expectations of electrostatics (qualitatively) and molecular solvation models (quantitatively) for small solutes. On the contrary, this scaling changes dramatically for large cavities, with the threshold cavity size in approximately the same range as the threshold solute/solvent size ratio observed for hydrophobic solvation. It turns out that the core of the solute becomes nonpolar with its growing size much faster than is normally anticipated. We will start our discussion with formulating the general results of the Gaussian solvation thermodynamics and then proceed to the outcome of computer simulations.

II. THERMODYNAMICS OF ELECTROSTATIC SOLVATION

By definition, electrostatic component μ_{0s} of the chemical potential of solvation is given by the ratio of two partition functions: One including the electrostatic solute-solvent interaction potential V_{0s} and one including nonelectrostatic solute-solvent interactions and all interactions between the solvent particles. All of these latter interactions are incorporated in the Hamiltonian H_0, while the overall Hamiltonian of the solute-solvent system is H_0+V_{0s}. The relation for μ_{0s} is then

$$e^{-\beta\mu_{0s}(\beta)} = Q(\beta)^{-1} \int e^{-\beta V_{0s}-\beta H_0} d\Gamma, \tag{1}$$

where

$$Q(\beta) = \int e^{-\beta H_0} d\Gamma. \tag{2}$$

Here, we use subscript "0" for the solute and subscript "s" for the solvent, $d\Gamma$ denotes integration over the system phase space, and β is the inverse temperature. Equation (1) can be conveniently rewritten in terms of the product of the Boltzmann distribution of finding the solute-solvent energy $\epsilon = V_{0s}$ and the probability density $P(\epsilon,\beta)$,

$$e^{-\beta\mu_{0s}(\beta)} = \int P(\epsilon,\beta) e^{-\beta\epsilon} d\epsilon, \tag{3}$$

where

$$P(\epsilon,\beta) = Q(\beta)^{-1} \int \delta(\epsilon - V_{0s}) e^{-\beta H_0} d\Gamma. \tag{4}$$

Equation (3) is exact and it states that all the thermodynamic information required to understand electrostatic solvation is contained in the statistics of the electrostatic interaction energy $\epsilon = V_{0s}$ when the solvent is actually not polarized by this potential; $V_{0s}=0$ for the Hamiltonian H_0.

The approximation that we will adopt in our formalism, which is supported by our present simulations and data from other groups [23–25], is to assume that the distribution function $P(\epsilon,\beta)$ is a Gaussian function with zero average

$$P(\epsilon,\beta) \propto \exp\left(-\frac{\epsilon^2}{2\sigma^2(\beta)}\right). \tag{5}$$

The approximation of zero average is the reflection of the fact that no specific orientation of the solvent dipoles is created around a nonpolar solute. This approximation is not necessarily always correct [9,26,27], but is insignificant for most of our development since a nonzero average, if it exists, can always be incorporated as a linear shift of ϵ. What is the most significant property for our analysis is the magnitude and temperature dependence of the Gaussian width $\sigma^2(\beta)$.

Within the Gaussian approximation for the electrostatic fluctuations around a nonpolar solute the solvation thermodynamics gains a simple and physically transparent form. The chemical potential of electrostatic solvation is

$$\mu_{0s} = -(\beta/2)\sigma^2(\beta). \tag{6}$$

In addition, one can determine the energy e and entropy s of electrostatic solvation

$$e = \langle V_{0s}\rangle + \Delta e_{ss},$$

$$Ts = \frac{\langle V_{0s}\rangle}{2} + \Delta e_{ss}. \tag{7}$$

In this equation, $\langle V_{0s}\rangle$ is the average solute-solvent electrostatic interaction energy when the full solute-solvent interaction is turned on and the system Hamiltonian is $H=H_0+V_{0s}$. From Eqs. (6) and (7),

$$\langle V_{0s}\rangle = -\beta\sigma^2(\beta). \tag{8}$$

The term Δe_{ss} in Eq. (7) determines the change in the interaction energy between the solvent molecules induced by electrostatic solute-solvent interaction. This energy term is identically equal to the corresponding contribution to the solvation entropy, $T\Delta s_{ss}=\Delta e_{ss}$, so that Δe_{ss} cancels out in the solvation chemical potential which is determined by the solute-solvent interaction thermodynamics only [28,29]. The term Δe_{ss} can be calculated by either taking the temperature derivative of the Gaussian width $\sigma^2(\beta)$ or from a third-order correlation function

$$\Delta e_{ss} = -\frac{\beta^2}{2}\frac{\partial\sigma^2}{\partial\beta} = (\beta^2/2)\langle \delta V_{0s}^2 \delta H_0\rangle_0. \tag{9}$$

In Eq. (9), the average $\langle\cdots\rangle_0$ is over an ensemble of a nonpolar solute in equilibrium with the solvent, collectively described by the Hamiltonian H_0. In addition, $\delta V_{0s}=V_{0s}-\langle V_{0s}\rangle_0$ and $\delta H_0=H_0-\langle H_0\rangle_0$ are the deviations from the average values determined on the same unpolarized ensemble.

III. SIMULATIONS AND DATA ANALYSIS

While the equations presented in Sec. II are generally applicable to an arbitrary solute, we will use numerical Monte Carlo (MC) simulations [3] to determine the statistics of fluctuations produced in spherical cavities carved from a

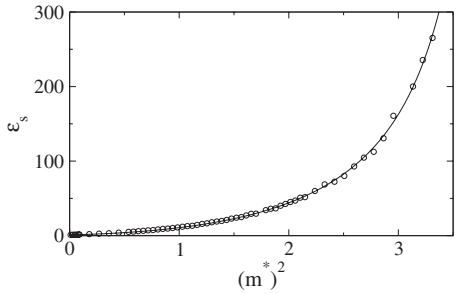

FIG. 1. Dielectric constant ϵ_s of the liquid of dipolar hard spheres vs the dipolar parameter $(m^*)^2=\beta m^2/\sigma^3$; $\rho^*=0.8$. The solid line represents the Padé approximation of the simulation data: $\epsilon_s(x)=(1+a_1x+a_2x^2)/(1+b_1x+b_2x^2)$ with $a_1=2.506$, $a_2=3.057$, $b_1=-0.180$, $b_2=-0.008\,65$ and $x=(m^*)^2$. The dielectric constants were calculated from *NVT* MC simulations of the homogeneous liquid of dipolar hard spheres using the Neumann [30] correction for the cutoff of dipolar interactions treated by the reaction-field formalism.

liquid of dipolar hard spheres (see Appendix A for the description of the simulation protocol). The fluid of dipolar hard spheres leaves out many important properties of real liquids, most notably van der Waals forces and higher order multipoles. However, it allows a significant simplification of the solvation thermodynamics since all physical properties of the solvent are expressed in terms of only two parameters, the reduced density $\rho^*=\rho\sigma^3$ and the reduced dipole moment $(m^*)^2=\beta m^2/\sigma^3$, where m is the dipole moment and σ is the diameter of the dipolar particles. Since the reduced density is fixed at $\rho^*=0.8$ in our simulations, our results are fully defined in terms of two parameters: The reduced cavity radius R_0/σ and the polarity parameter $(m^*)^2$. The representation in terms of the dielectric constant ϵ_s can be easily achieved as well since these values are tabulated from our simulations as is shown in Fig. 1. The dielectric constants were calculated from Neumann's formalism [30] as described in detail in Ref. [31].

We will also limit our consideration to two types of electrostatic multipoles most commonly studied in theories and applications of solvation, point ion and point dipole [6,7,24]. In both cases, the corresponding multipole is placed at the center of the spherical cavity. The solute-solvent interaction potential is then given as $V_{0s}=q_0\varphi_s$ in the case of an ion and $V_{0s}=-\mathbf{m}_0\cdot\mathbf{E}_s$ for a dipole. In these relations, q_0 and m_0 are the charge and dipole moment of the probe multipole and φ_s and $\mathbf{E}_s$ are, respectively, the potential and electric field produced by the solvent at the multipole position.

The main parameter entering the Gaussian model of solvation that we want to monitor is the Gaussian width $\sigma^2(\beta)$. Since we want to deal with dimensionless quantities, we will in fact calculate the temperature reduced parameter

$$\Gamma=\beta^2\sigma^2(\beta)=\beta^2\langle(\delta V_{0s})^2\rangle_0. \tag{10}$$

Since this parameter depends on the multipolar character of the solute, it is convenient to take this information out and consider the parameter Δ such that the temperature-reduced electrostatic energy of the solute is taken out as a multiplier

$$\Gamma=w\Delta. \tag{11}$$

Here, the electric field of the multipole (charge or dipole) E_0 is used to define the electrostatic energy

$$w=(\beta/8\pi)\int_\Omega E_0(\mathbf{r})^2d\mathbf{r}, \tag{12}$$

where the integral is taken over the solvent volume Ω outside the spherical cavity.

The parameter w is equal to $\beta q_0^2/(2R_0)$ for an ion and $\beta m_0^2/(3R_0^3)$ for a dipole, where R_0 is the cavity radius. Therefore, one can calculate the parameter Δ according to the following relations in case of an ionic (subscript "*i*") or dipolar (subscript "*d*") solute

$$\Delta_i=2\beta R_0\langle(\delta\phi_s)^2\rangle_0,$$

$$\Delta_d=\beta R_0^3\langle(\delta\mathbf{E}_s)^2\rangle_0. \tag{13}$$

Similarly, we will introduce the reduced parameter Δ_{ss} for the components of the internal energy and entropy arising from the alteration of the solvent-solvent interactions, $\beta\Delta\epsilon_{ss}=w\Delta_{ss}$,

$$\Delta_{ss}^i=\beta^2R_0\langle(\delta\phi_s)^2\delta H_0\rangle_0,$$

$$\Delta_{ss}^d=(\beta^2R_0^3/2)\langle(\delta\mathbf{E}_s)^2\delta H_0\rangle_0. \tag{14}$$

A few analytical results from standard electrostatics [4] can be used as benchmarks in calculating Δ_i and Δ_d. The continuum electrostatics of Born [6] and Onsager [7] equations gives the response functions $\Delta_{i,d}$ depending only on the dielectric constant ϵ_s of the dipolar liquid,

$$\Delta_i=2\left(1-\frac{1}{\epsilon_s}\right) \tag{15}$$

and

$$\Delta_d=6\frac{\epsilon_s-1}{2\epsilon_s+1}. \tag{16}$$

In addition, several microscopic relations have been derived based on different formulations of the liquid-state theory. A closed-form equation for ion solvation is provided by the Ornstein-Zernike integral equations for the ion-dipole mixture solved in the mean-spherical approximation (MSA) [32],

$$\Delta_i=\frac{2R_0}{R_0+\Lambda_L}\left(1-\frac{1}{\epsilon_s}\right). \tag{17}$$

In this equation, $\Lambda_L=3\sigma\xi/(1+4\xi)$ is the correlation length of the longitudinal polarization fluctuations of a dipolar liquid and ξ is the MSA polarity parameter [33].

An analogous MSA solution exists for a mixture of dipolar particles of different size [34], which gives the parameter Δ_d. Truncated perturbation expansions [35] are however known to work better in this case with the result [31,36]

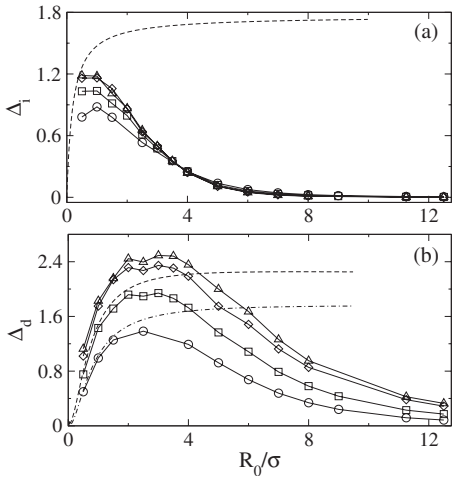

FIG. 2. Δ_i (a) and Δ_d (b) vs the cavity radius R_0 for $(m^*)^2=0.5$ (circles), 1.0 (squares), 2.0 (diamonds), and 3.0 (up-triangles). The dashed line in (a) gives the result of Eq. (17) for $m^*=1.0$. The dashed-dotted and dashed lines in (b) show the application of Eq. (18) at $(m^*)^2=0.5$ and 1.0, respectively; $N=1372$.

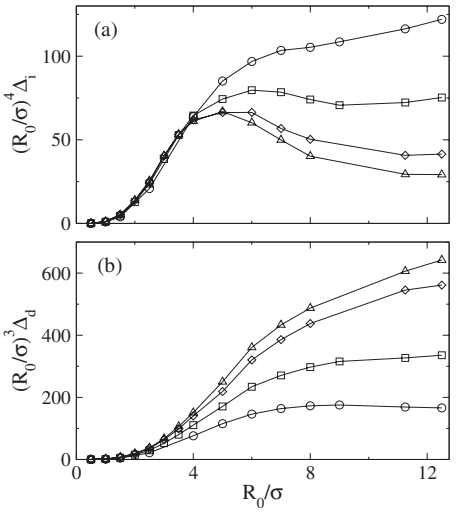

FIG. 3. $(R_0/\sigma)^4\Delta_i$ (a) and $(R_0/\sigma)^3\Delta_d$ (b) vs the cavity radius R_0 for $(m^*)^2=0.5$ (circles), 1.0 (squares), 2.0 (diamonds), and 3.0 (up-triangles); $N=1372$.

$$\Delta_d = 6\left(\frac{R_0}{R_{\text{eff}}}\right)^3 \frac{y}{1+\kappa(y,r_{0s})y\sigma^3 I_{0s}^{(3)}/R_{\text{eff}}^3}. \tag{18}$$

Here, $r_{0s}=R_0/\sigma+0.5$ is the reduced distance of the closest approach of the liquid molecules to the cavity and $y=(4\pi/9)\beta m^2\rho$ is the standard density of dipoles in the dipolar liquid [5], ρ is the liquid number density. In addition, $I_{0s}^{(3)}(r_{0s},\rho^*)$ is the three-particle perturbation integral which is a function of the liquid density and r_{0s} and $R_{\text{eff}}(r_{0s},\rho^*)$ is the effective radius of the cavity

$$R_{\text{eff}}^{-3}(r_{0s},\rho^*) = 3\int_0^\infty \frac{dr}{r^4} g_{0s}^{(0)}(r). \tag{19}$$

In this equation $g_{0s}^{(0)}(r)$ is the hard-sphere distribution function of the liquid particles as a function of the distance r from the cavity center. All functions $R_{\text{eff}}(r_{0s},\rho^*)$, $I^{(3)}(r_{0s},\rho^*)$, and $\kappa(y,r_{0s})$ are given analytically in terms of the corresponding parameters in Ref. [36].

IV. RESULTS

Our simulations have produced an unexpected result. We found that the scalings of the electrostatic fluctuations, and of the corresponding chemical potentials, with the cavity size do not follow the predictions of either the continuum electrostatics or microscopic solvation models in the limit of large cavities. The results are shown in Fig. 2. As is seen, the potential variance $\langle(\delta\varphi_s)^2\rangle$ decays much faster than the expected $1/R_0$ scaling [Eqs. (13) and (15)] for all cavities greater than the size of the solvent particle. The large cavity scaling does not follow any universal law, but instead depends on polarity of the liquid (parameter m^*, Fig. 3). For the range of liquid polarities studied here, the large-cavity scaling of $\langle(\delta\varphi_s)^2\rangle$ is approximately $1/R_0^{4-6}$ [Fig. 3(a)].

Fluctuations of the electric field at the cavity center do not deviate that dramatically from the traditional expectations, but the parameter Δ_d still decays to zero [Fig. 2(b)] instead of leveling off as suggested by Eqs. (16) and (18). In fact, Δ_d follows Eq. (18) quite well up to the cavity size about 4–5 times larger than the liquid particle, but then starts to drop following qualitatively the trend seen for the potential fluctuations. Continuum electrostatics [Eqs. (15) and (16)] fails both qualitatively and quantitatively for the electrostatic fluctuations of either the potential or the electric field.

One can understand the appearance of the $1/R_0^4$ scaling for Δ_i from the following qualitative arguments. A charge placed at the cavity center generates dipolar polarization $P \propto \alpha/r^2$ in the medium, where $\alpha=\beta m^2/3$. If this polarization field propagates through the entire liquid, one needs to integrate $-PE \propto \alpha/r^4$ over the liquid volume, which results in $1/R_0$ scaling for the interaction energy. If, on the contrary, the polarization is screened by the liquid layers subsequent to the first polarized layer, one gets an alternative scaling of $1/R_0^4$ arising from the first solvation layer only. The exact microscopic mechanism behind the solvent reorganization at the interface is unknown, but these simple arguments suggest that the solvent at the surface of a large cavity has enough configurational flexibility to reorganize itself to effectively screen the penetration of the field into the liquid. The same arguments would suggest the scaling $1/R_0^6$ for the variance of the field fluctuations. This scaling seems to apply to low-polarity liquids, but the decay slows down to $1/R_0^5$ for higher polarities [Fig. 3(b)] pointing to a more correlated response of the dipoles in the first two solvation layers.

With the dramatic failure of some very basic expectations regarding electrostatic fluctuations, as is shown in Fig. 2, one wonders if the Gaussian approximation for the distribution of the electrostatic interaction energies [Eq. (5)] fails for large cavities. We have performed extensive tests of the Gaussian statistics of the electrostatic fluctuations as summarized in Appendix B. In particular, we have looked at the parameter δ_G describing deviations from the Gaussian statistics for both potential and field fluctuations,

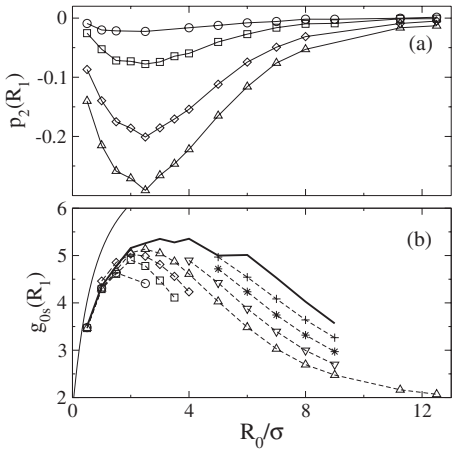

FIG. 4. (a): Orientational order parameter [Eq. (21)] vs the cavity size for different polarities of the solvent, $(m^*)^2=0.5$ (circles), 1.0 (squares), 2.0 (diamonds), and 3.0 (up-triangles); $N=1372$. (b) Contact value of the cavity-solvent radial distribution function at $r=R_1=R_0+\sigma/2$ and $(m^*)^2=1.0$ vs the cavity radius. Shown are the results for different number of particles in the simulation box $N=256$ (circles), 500 (squares), 864 (diamonds), 1372 (up-triangles), 2048 (down-triangles), 2916 (stars), 4000 (pluses). Extrapolation to $N\rightarrow\infty$ is shown by the bold solid line. The dashed lines connect the points. The thin solid line gives the contact value of the distribution function in the hard-spheres mixture from Ref. [37].

$$\delta_G = \frac{\langle (\delta V_{0s})^4 \rangle_0}{\langle (\delta V_{0s})^2 \rangle_0^2} - 3. \tag{20}$$

This parameter was found to be around zero, as expected for the Gaussian statistics, within about 5% of the simulation uncertainties (see Appendix B). In addition, we have studied the dependence of the second field cumulants on the magnitude of the solute dipole placed at the cavity center, and the results are consistent with the expectations from the Gaussian solvation model. All of these tests have shown that the Gaussian approximation is reliable within simulation uncertainties and the observed change in the scaling should be attributed to a dramatic restructuring of the cavity interface beyond some crossover cavity size.

In order to gain more insight into the origin of the observed crossover in the scaling with the cavity size, we have calculated two local parameters related to the orientational and density structure of the liquid-cavity interface. Figure 4(a) shows the second-rank orientational order parameter of the permanent dipoles in the first solvation shell at the cavity surface,

$$p_2(r) = \left\langle \sum_j P_2(\hat{\mathbf{r}}_j \cdot \hat{\mathbf{e}}_j)\, \delta(\mathbf{r}_j - \mathbf{r}) \right\rangle. \tag{21}$$

Here, $P_2(x)$ is the second Legendre polynomial, $\hat{\mathbf{r}}_j=\mathbf{r}_j/r_j$ is the unit vector in the direction of the liquid particle j, and $\hat{\mathbf{e}}_j$ is the unit vector along its dipole moment. The orientational order parameter shown in Fig. 4(a) is calculated by limiting the distance r to the liquid particles residing in the cavity's first solvation shell. The parameter indicates preferential orientation of the first-shell dipoles parallel to the interface. In contrast, the first-rank orientational parameter, based on the first-order Legendre polynomial, is identically zero thus implying that there is no net dipolar polarization at the cavity surface. This result is distinct from the water surface where water's large quadrupole moment is responsible for the asymmetry [9].

As the cavity gets larger the solvent dipoles find it more energetically favorable to orient parallel to the interface, as was also observed for 2D dipolar liquids [38], for water at cavity surfaces [39] and liquid-vapor interfaces [9], and for interfaces of dipolar liquids [40]. In-plane orientation of dipoles is also preferable for water at a hydrophobic surface [41]. However, this preferential orientational order starts to dissolve with a further increase of the cavity size, after gaining maximum for the cavity about 5 times larger than the solvent particle. This decay is related to the onset of softening of the first solvation shell indicated by the contact value of the pair cavity-solvent distribution function shown in Fig. 4(b).

The contact value of the pair distribution function first rises as expected for a hard-sphere solute in a fluid of densely packed hard spheres [37] [thin solid line in Fig. 4(b)], but then starts to drop. This drop sets in at approximately the same cavity size $R_0/\sigma\simeq 2-2.5$ as both the downward turn of the orientational order parameter and the onset of deviations of the electric field fluctuations from the traditional predictions [position of the maximum in Fig. 2(b)]. We therefore can conclude that the observed change in the character of the electrostatic fluctuations is related to the softening of the liquid-cavity interface, which also weakens the energetic push for a specific dipolar order. This interfacial softening appears to be a general property of liquids with attractive interactions [16].

The position of the maximum of the solute-solvent distribution function defines a natural length scale of the problem beyond which the character of the electrostatic fluctuations changes from volume dominated to surface dominated, with a corresponding change in the scaling. One cannot escape the analogy between this observation and the transition from the volume to surface dominated energetics of cavity formation in water [12,13,18]. The turnover is commonly explained by the change in the network of water's hydrogen bonds which is mostly preserved around small solutes, but become disrupted by solutes of the size larger than the turnover length. There are no hydrogen bonds for hard-sphere dipoles studied here, but there is a change in the character of the dipolar correlations at the turnover, as characterized by the second-rank orientational parameter. It is therefore not entirely clear if the same physics is behind the turnover of hydrophobic solvation (cavity formation) and electrostatic dipolar solvation. What is however clear is that the turnover length seen in the present simulations, $R_0/\sigma\simeq 3-4$ (Fig. 4), is noticeably higher than the maximum of the contact density of water at around $R_0/\sigma\simeq 1$ first proposed by Pierotti and Stillinger [42] and more recently found in numerical simulations [14,18]. Since a similar value of the contact density maximum was found for cavities in Lennard-Jones (LJ) fluids [16], the difference with our observations might originate from LJ attractions in these two force-field fluids absent from dipolar hard spheres studied here. If this conjecture is correct, the strength

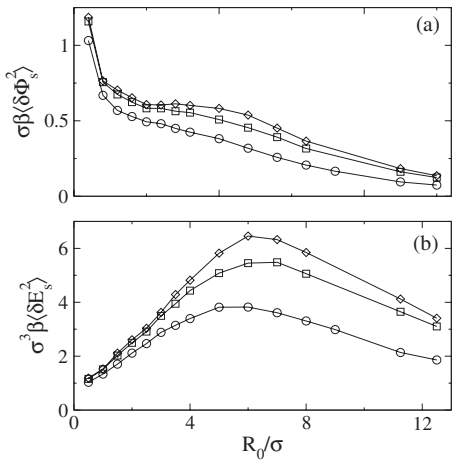

FIG. 5. $\sigma\beta\langle(\delta\varphi_s)^2\rangle$ (a) and $\sigma^3\beta\langle(\delta\mathbf{E}_s)^2\rangle$ (b) vs the cavity size for probe charge and dipole located the distance $\sigma/2$ from the cavity surface. The points refer to $(m^*)^2=1.0$ (circles), 2.0 (squares), and 3.0 (diamonds); $N=1372$.

of isotropic attractive forces between the solvent particles might alter the turnover length of electrostatic solvation by enhancing the interfacial softening.

That the decay of solvation energies is related to the interface softening is also seen from examining the fluctuations of the potential and field close to the cavity surface. Figure 5 shows the corresponding quantities for a point within the cavity kept one solvent radius $\sigma/2$ away from the interface once the cavity size is increased. Again, simple electrostatic arguments suggest that the solvation energetics should approach that for a probe charge or dipole next to an infinite dielectric wall. Depending on how the dielectric interface is defined, by the cavity boundary or by the distance of the closest approach, continuum electrostatics [4] predicts for $\sigma\beta\langle(\delta\varphi_s)^2\rangle$ the value between $(\epsilon_s-1)/(\epsilon_s+1)$ and $0.5(\epsilon_s-1)/(\epsilon_s+1)$. The observed dependence does seem to inflect to a plateau at the level consistent with this prediction at an intermediate cavity size, but then starts to decay. This decay is however much more gentle than in Fig. 2 indicating that the area next to the interface experiences a stronger solvent influence than the part of the hollow space closer to the cavity center.

In Fig. 6 we show the simulation results for the solvent-solvent component of the solvation entropy [Eq. (7)]. Within the Gaussian approximation, the ratio of the solvent-solvent solvation entropy, $Ts_{ss}=\Delta e_{ss}$, and the solute-solvent entropy, $Ts_{0s}=-\beta\sigma^2(\beta)/2$, is given as the ratio of the corresponding reduced response functions

$$\chi_s=-\frac{s_{ss}^{i,d}}{s_{0s}^{i,d}}=\frac{2\Delta_{ss}^{i,d}}{\Delta_{i,d}}. \tag{22}$$

As is seen, for both the ionic and dipole solvation, there is a compensation between ordering of the solvent by the solute, expressed by the always negative s_{0s}, and disordering of the solvent structure, expressed by the positive s_{ss}. This compensation is however far from complete, in contrast to a much stronger compensation suggested for aqueous solvation [43,44]. The overall entropy of electrostatic solvation is therefore negative. Since the parameter χ_s in Eq. (22) depends weakly on the cavity size, the dramatic change in the character of solvation found here for $\sigma^2(\beta)$ will be reflected in both the enthalpy and entropy of electrostatic solvation which are often better accessible experimentally than solvation free energies [44]. Very little is currently known about the magnitude of χ_s [44], in particular for large solutes. Our recent MD simulations of the redox entropy of hydrated metalloprotein plastocyanin [45] have produced $\chi_s\simeq 0.4$ ($R_0/\sigma\simeq 5.8$). Since that protein carries a negative charge, this value is consistent with the results for ionic solutes in Fig. 6, although it is not clear if the Gaussian approximation is applicable to the protein electrostatics.

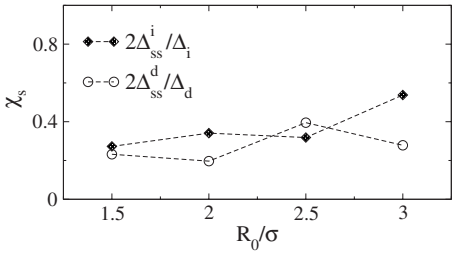

FIG. 6. The ratio of the solute-solvent and solvent-solvent components of the solvation entropy [Eq. (22)] vs the cavity radius calculated for charge (diamonds) and dipole (circles) probe multipoles from MC configurations.

V. DISCUSSION

In this paper we have studied polar solvation starting from Eq. (3) which states that all the information required to calculate solvation thermodynamics is contained in the distribution $P(\epsilon)$ of electrostatic interaction energies around a fictitious solute with the solute-solvent electrostatic coupling switched off. This equation is exact and the approximation adopted here is that the distribution function $P(\epsilon)$ is a Gaussian. The distribution $P(\epsilon)$ can generally be written as

$$P(\epsilon)\propto\exp[\beta\omega(\epsilon)] \tag{23}$$

and the integral over ϵ in Eq. (3) can be taken by the steepest descent around the stationary point ϵ_0 defined by the condition $\omega'(\epsilon_0)=1$. The Gaussian approximation is then equivalent to assuming that all terms except the linear one can be dropped from the series expansion of $\omega'(\epsilon)$ in powers of $(\epsilon-\epsilon_0)$.

Our simulations have not identified any significant deviations from the Gaussian statistics of the solute-solvent interaction energy. Extensive simulations of solvation of ionic and dipolar solutes over the last decades [23–25,46] have also come to the conclusion that the Gaussian picture is an accurate one implying that $P(\epsilon)$ is globally a Gaussian function. However, one can argue that our cavity setup does not allow us to sample sufficiently around ϵ_0 and thus we could not assess the deviations from the Gaussian statistics. While that might be true for strong solute-solvent interactions, for which a significant database pointing to the contrary exists [23,25,46], energy ϵ_0 is expected to decrease with increasing the cavity size and the Gaussian approximation is expected

to become increasingly accurate (as indeed seen from comparing Figs. 8 and 9 in Appendix B). However, it is in this range of large cavities, essentially neglected by previous studies of electrostatic solvation, that we found the most dramatic deviations from the traditional expectations.

The main finding of this study is that electrostatic solvation by polar liquids changes its character at the cavity size of about 4–5 times larger than the size of the solvent particle. The regime of small cavities can be reasonably understood by applying the currently available molecular solvation models and, in particular, the results for the electric field fluctuations (probe dipole) are in a very good quantitative agreement with the results of perturbation solvation models. In contrast, solvation in large cavities is dramatically different and cannot be described by traditional solvation models.

What we have observed here is a dramatic decay of the solvation strength in the center of the cavity, much faster than expected from both the continuum electrostatics and microscopic solvation models. For instance, the variance of the electrostatic potential decays as $1/R_0^{4-6}$ instead of the expected $1/R_0$ scaling. We suggest that the scaling turnover comes from the changing character of electrostatic solvation from volume dominated to surface dominated. The core of a growing hollow cavity thus becomes nonpolar much faster than previously anticipated. What it practically means is that there is very little solvation stabilization for charges inside a large mesoscale object. This might be a reason why natural systems requiring hydration of large molecular assemblies (proteins, etc.) rely on solvation of surface charges for which much slower decay of solvating power was found here. For the problem of protein folding, this observation implies a very strong driving force for placing ionized residues and cofactors stabilizing protein solvation closer to the interface.

ACKNOWLEDGMENTS

This research was supported by the National Science Foundation (Grant No. CHE-0616646). CPU time for parallel MC simulations was provided by ASU's Center for High Performance Computing.

APPENDIX A: SIMULATION PROTOCOL AND RESULTS

MC simulations were performed with the standard *NVT* Metropolis algorithm. The initial configuration was constructed starting from an fcc lattice of liquid hard spheres of diameter σ and density $\rho^*=0.8$. The hard-sphere solute or cavity was then "grown" in the center of the simulation box by increasing the initial cavity diameter of 0.5σ with an 0.002σ increment, adjusting σ to ensure constant density, and moving and rotating the solvent particles according to the Metropolis algorithm. After the solute or cavity was constructed, the initial configuration was created from 10^5-10^6 parallel steps (using OpenMPI) producing different initial configurations for each processor. The subsequent runs were then carried out on each processor separately thus minimizing interprocessor communications. To guarantee the Markovian statistics, the random number generators used in the MC moves were seeded independently between the processors. This implementation has resulted in a linear scaling of the program output with the number of processors. The production runs of $(1-5)\times 10^6$ steps were performed on 10 processors per $(m^*)^2$ per cavity size.

The simulation protocol employed the minimum image convention and the reaction-field correction [3] for the cutoff of dipolar interactions at one-half of the cubic simulation box. Ewald sums [47] were also tested and gave results identical within simulation uncertainties. The reaction-field correction was preferred due to better performance. The dependence on the simulation box size was carefully checked in particular since growing cavity required larger number of liquid particles to eliminate finite-size effects. The number of particles N was varied in the range $N=108$, 256, 500, 864, 1372, 2048, 2916, and 4000 depending on the cavity size. The representative results for Δ_i and Δ_d listed in Table I were obtained by averaging over several simulation runs with different box sizes and also by extrapolating the plots of corresponding values vs $1/N$ to the $N\to\infty$ limit. The system size dependence does not affect any qualitative conclusions we make here. Since extrapolation to $N\to\infty$ creates a scatter of points, the results presented in the plots refer to a given number of particles in the simulation cell.

APPENDIX B: TESTS OF THE GAUSSIAN APPROXIMATION

The Gaussian approximation is a central part of our thermodynamic arguments and so we have done extensive tests of its applicability. Figure 7 shows the simulated values of the parameter δ_G from Eq. (20) vs the solvent dielectric constant [Fig. 7(a)] and the cavity size [Fig. 7(b)]. This parameter is close to zero, as expected for a Gaussian noise, within the simulation uncertainties. An additional test of the Gaussian statistics of electrostatic fluctuations comes from the dependence of the potential and field variances on the magnitude of the test multipole located at the cavity center. Since the chemical potential of solvation is given by the variance of the solute-solvent interaction potential [Eq. (6)], it is a quadratic function of the magnitude of a test multipole. This result, known as the linear response approximation [24], suggests that the response function, obtained as the second derivative of μ_{0s} in the corresponding multipole, does not depend any more on the multipole's magnitude. It also implies that $\Delta_{i,d}$ can be obtained either from simulations of empty cavities or from simulations involving actual multipoles inside the cavity. In this second route, the chemical potential of solvation and corresponding parameters $\Delta_{i,d}$ are calculated from the average solute-solvent interaction energy by using Eq. (8). Such simulations involving the probe charge are not straightforward due to the breakdown of the system neutrality and the related difficulty of using the Ewald sums [47,48]. We therefore have done simulations of point dipoles of varying magnitude placed at the cavity's center. The values of Δ_d have been calculated from the average interaction energy for the cavity size above the threshold seen in Fig. 2(b), $R_0/\sigma=9.0$, and the simulation box containing $N=2048$ solvent particles (Fig. 8).

TABLE I. Values of Δ_i and Δ_d for $(m^*)^2=0.5,1.0,2.0,3.0$ ($\epsilon_s=3.63,8.51,29.9,93.7$). Extrapolations (ext.) were performed with $N=108,256,500,864,1372,2048,2916,4000$ liquid particles in the simulation box when available by linearly fitting $\Delta_{i,d}$ vs $1/N$ and taking the intercept. The system sizes used for the extrapolations are given in the footnotes.

		$(m^*)^2$							
		0.5		1.0		2.0		3.0	
R_0/σ	N	Δ_i	Δ_d	Δ_i	Δ_d	Δ_i	Δ_d	Δ_i	Δ_d
0.5	1372	0.781	0.498	1.031	0.753	1.158	1.020	1.185	1.126
	ext.[a]	0.814	0.572	1.052	0.761	1.210	1.030	1.265	1.153
1.0	1372	0.892	1.001	1.035	1.431	1.184	1.801	1.240	1.939
	ext.[b]	0.863	1.009	1.050	1.449	1.171	1.768	1.198	1.854
1.5	1372	0.778	1.256	0.936	1.760	1.058	2.137	1.073	2.286
	ext.[c]	0.834	1.292	1.011	1.772	1.084	2.112	1.103	2.238
2.0	1372			0.795	1.918	0.859	2.314	0.866	2.444
	ext.[c]			0.862	1.965	0.844	2.300	0.859	2.394
2.5	1372	0.533	1.384	0.632	1.955	0.670	2.365	0.666	2.513
	ext.[c]	0.619	1.491	0.692	2.079	0.695	2.470	0.710	2.627
3.0	1372			0.475	1.941	0.499	2.345	0.499	2.492
	ext.[d]			0.612	2.122	0.550	2.468	0.556	2.587
3.5	1372			0.352	1.864	0.355	2.307	0.355	2.482
	ext.[d]			0.459	2.129	0.376	2.539	0.375	2.578
4.0	1372	0.249	1.191	0.252	1.723	0.242	2.188	0.239	2.356
	ext.[e]			0.495	2.186	0.528	2.597	0.533	2.699
5.0	1372	0.136	0.927	0.124	1.431	0.112	1.830	0.107	2.000
	ext.[f]	0.299	1.393	0.310	2.004	0.251	2.388	0.246	2.556
6.0	1372	0.075	0.675	0.061	1.084	0.051	1.483	0.046	1.670
	ext.[g]	0.298	1.449	0.296	2.061	0.236	2.484	0.233	2.553
7.0	1372	0.043	0.478	0.033	0.789	0.024	1.124	0.021	1.263
	ext.[g]	0.192	1.233	0.183	1.834	0.133	2.203	0.125	2.373
8.0	1372	0.026	0.338	0.018	0.581	0.012	0.855	0.010	0.952
	ext.[g]	0.128	1.003	0.114	1.540	0.054	1.790	0.048	2.004
9.0	1372	0.017	0.241	0.011	0.433				
	ext.[g]	0.087	0.803	0.071	1.258				
10.0	4000			0.036	0.830	0.029	1.176	0.025	1.304
11.25	1372	0.0073	0.119	0.0045	0.230	0.0025	0.383	0.0018	0.426
12.5	1372	0.0050	0.085	0.0031	0.172	0.0017	0.287	0.0012	0.329

[a]108, 256, 500, 1372, 2048.
[b]108, 256, 500, 864, 1372.
[c]256, 500, 864, 1372.
[d]500, 864, 1372.
[e]864, 1372, 2048.
[f]500, 864, 1372, 2048, 2916, 4000.
[g]1372, 2048, 2916, 4000.

Figures 8(b) and 8(c) also present the corresponding contact values of the cavity-solvent pair distribution function $g_{0s}(R_1)$ and the orientational order parameter $p_2(R_1)$. The response function Δ_d stays constant almost in the entire range of m_0 studied, starting to rise when the dipole inside the cavity exceeds the solvent dipole by three orders of magnitude. This rise is a reflection of a change in the microscopic structure of the interface as the first solvation shell gets stiffer under the pull of the solute dipole field and the first-shell dipoles start to reorient along the field of the solute dipole. The observed changes in the functions $g_{0s}(R_1)$ and $p_2(R_1)$ are, however, much greater than the corresponding change in Δ_d testifying to the collective nature of the solvent dipolar response effectively averaging out the local changes in the structure of the first solvation shell.

In Fig. 9 we show the same data as in Fig. 8 obtained at a much smaller cavity size $R_0/\sigma=1.5$. Here, the change in the local structure with increasing the solute dipole is more pronounced, and Δ_d starts to show a dependence on the magnitude of the probe dipole signalling the onset of nonlinear

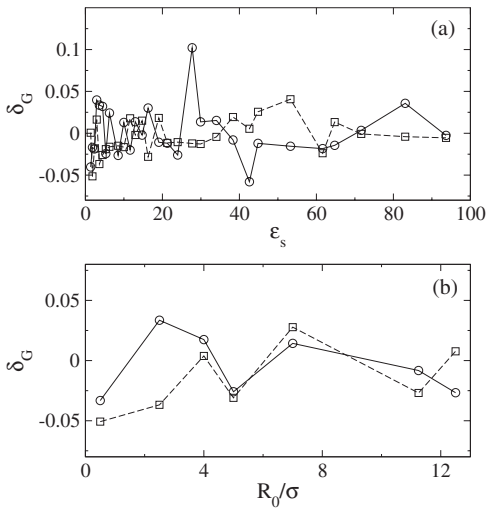

FIG. 7. Response function Δ_d (a), contact value of the cavity-solvent pair distribution function $g_{0s}(R_1)$ (b), and the orientational order parameter of the dipoles in the first solvation shell $p_2(R_1)$ (c) vs the magnitude of the solute dipole at the cavity center m_0. Points are the results of MC simulations with $R_0/\sigma=9.0$, $(m^*)^2=1.0$, and $N=2048$. The lines connect the simulation points.

solvation effects. The variation in the response function is still mostly within 10% of its value, which can be accounted for by nonlinear extensions of dipolar solvation models [31]. We need to stress, however, that the Gaussian approximation appears to be robust for large cavities which are of main interest for us here. Figures 8 and 9 in fact demonstrate that when a dipole is inserted at the center of a large cavity, the standard solvation models will fail to reproduce the results of

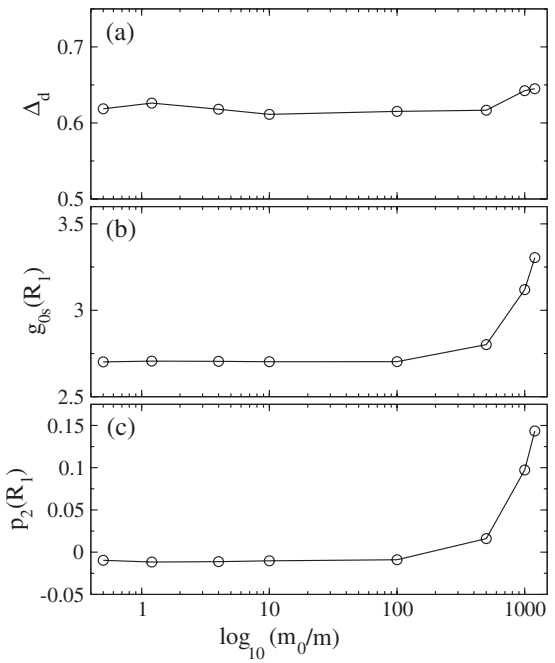

FIG. 8. Parameter δ_G describing deviations from Gaussian statistics [Eq. (20)] vs ϵ_s (a) and R_0 (b). Points represent probe ions (circles) and probe dipoles (squares) for $R_0/\sigma=2.5$ (a) and $(m^*)^2=0.5$ (b).

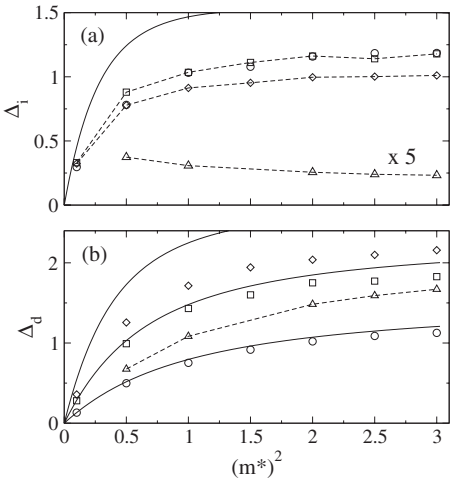

FIG. 9. Δ_i (a) and Δ_d (b) as functions of $(m^*)^2$ for $R_0/\sigma=0.5$ (circles), 1.0 (squares), 1.5 (diamonds), and 6.0 (up-triangles). The solid line in (a) shows the result of using Eq. (17) at $R_0/\sigma=1.0$. The solid lines in (b) show the result of Eq. (18) for $R_0/\sigma=0.5$, 1.0, and 6.0 (from down to up); the dashed lines in (a) and (b) connect the points. The data for Δ_i at $R_0/\sigma=6.0$ (up-triangles) in (a) have been multiplied by a factor of 5 to bring them to the scale of the plot. The simulation points were obtained at $N=1372$ dipolar hard spheres in the box.

the present numerical simulations. A weak sensitivity of the response functions to the magnitude of the solute dipole also suggests that the crossover behavior in the character of electrostatic fluctuations and the corresponding crossover length will not be significantly affected by the presence of a solute multipole unless the solute-solvent interactions significantly exceed the solvent-solvent interactions at the cavity size when the crossover occurs. The main conclusion of this set of simulations is that our results obtained from fluctuations inside empty cavities are transferable to more often encountered problems when dipoles and charges reside inside molecular or mesoscopic objects dissolved in polar liquids.

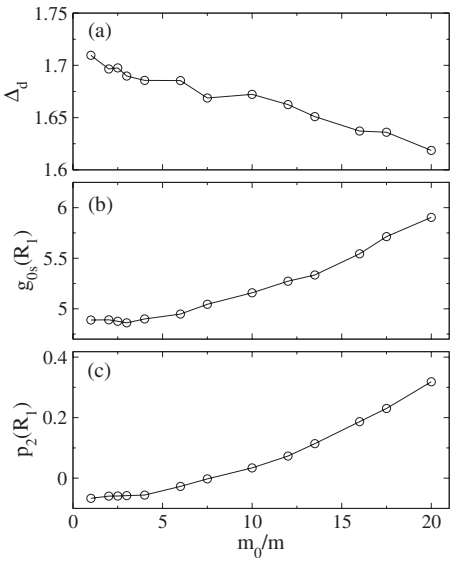

FIG. 10. Same as in Fig. 8 for $R_0/\sigma=1.5$; $N=864$.

We next turn to the dependence of the cavity response functions on liquid polarity. Figure 10(a) shows the dependence of Δ_i on the solvent dipole moment. For small cavities, when the standard scaling with the cavity size is expected to apply, the dependence of Δ_i on polarity does not show a saturation predicted by the continuum electrostatics [Eq. (15)]. This saturation seems to set in for a slightly larger cavity, but, as seen for a still larger cavity, it is simply enroute to become a decreasing function of polarity for the largest cavities studied here. We can therefore conclude that there is no range of parameters where both the size scaling and the dependence on polarity predicted by the continuum electrostatics for the potential fluctuations are satisfied even at the qualitative level, not to mention the fact that the predicted values are significantly off.

The saturation of μ_{0s} at $\epsilon_s \to \infty$ predicted by the Onsager equation for dipole solvation [Eq. (16)] is never reached in our simulations. In contrast to the potential fluctuations, the variance of the field is a uniformly increasing function with increasing solvent dipole for all cavity sizes studied here. A similar trend, for a narrower range of parameters, was previously observed by us [46] and is manifested in solvation dynamics uniformly slower than continuum predictions [49]. The results for Δ_d from Eq. (18) are shown by the solid lines in Fig. 10(b). As expected, there is a good agreement between the microscopic theory and simulations for small cavities, but then the theory fails when the scaling of the solvation free energy with the cavity size changes and Δ_d turns downward as in Fig. 2(b).

[1] T. L. Beck, M. E. Paulaitis, and L. R. Pratt, *The Potential Distribution Theorem and Models of Molecular Solutions* (Cambridge University Press, Cambridge, 2006).
[2] J. P. Hansen and I. R. McDonald, *Theory of Simple Liquids* (Academic, Amsterdam, 2003).
[3] M. P. Allen and D. J. Tildesley, *Computer Simulation of Liquids* (Clarendon, Oxford, 1996).
[4] L. D. Landau and E. M. Lifshitz, *Electrodynamics of Continuous Media* (Pergamon, Oxford, 1984).
[5] C. J. F. Böttcher, *Theory of Electric Polarization* (Elsevier, Amsterdam, 1973), Vol. 1.
[6] M. Born, Z. Phys. **1**, 45 (1920).
[7] L. Onsager, J. Am. Chem. Soc. **58**, 1486 (1936).
[8] A. V. Marenich, C. J. Cramer, and D. G. Truhlar, J. Chem. Theory Comput. **4**, 877 (2008).
[9] V. P. Sokhan and D. J. Tildesley, Mol. Phys. **92**, 625 (1997).
[10] D. R. Martin and D. V. Matyushov, Europhys. Lett. **82**, 16003 (2008).
[11] A. A. Rashin, Prog. Biophys. Mol. Biol. **60**, 73 (1993).
[12] D. Chandler, Nature (London) **437**, 640 (2005).
[13] K. Lum, D. Chandler, and J. D. Weeks, J. Phys. Chem. B **103**, 4570 (1999).
[14] S. Rajamani, T. M. Truskett, and S. Garde, Proc. Natl. Acad. Sci. U.S.A. **102**, 9475 (2005).
[15] G. Hummer and S. Garde, Phys. Rev. Lett. **80**, 4193 (1998).
[16] D. M. Huang and D. Chandler, Phys. Rev. E **61**, 1501 (2000).
[17] A. C. Maggs and R. Everaers, Phys. Rev. Lett. **96**, 230603 (2006).
[18] H. S. Ashbaugh and L. R. Pratt, Rev. Mod. Phys. **78**, 159 (2006).
[19] T. Rudas, C. Schröder, and O. Steinhauser, J. Chem. Phys. **124**, 234908 (2006).
[20] M. V. Athawale, G. Goel, T. Ghosh, T. M. Truskett, and S. Garde, Proc. Natl. Acad. Sci. U.S.A. **104**, 733 (2007).
[21] N. Giovambattista, C. F. Lopez, P. J. Rossky, and P. G. Debenedetti, Proc. Natl. Acad. Sci. U.S.A. **105**, 2274 (2008).
[22] J. C. Rasaiah, S. Garde, and G. Hummer, Annu. Rev. Phys. Chem. **59**, 713 (2008).
[23] R. A. Kuharski, J. S. Bader, D. Chandler, M. Sprik, M. L. Klein, and R. W. Impey, J. Chem. Phys. **89**, 3248 (1988).
[24] J. Aqvist and T. Hansson, J. Phys. Chem. **100**, 9512 (1996).
[25] J. Blumberger and M. Sprik, J. Phys. Chem. B **109**, 6793 (2005).
[26] H. S. Ashbaugh, J. Phys. Chem. B **104**, 7235 (2000).
[27] D. S. Cerutti, N. A. Baker, and J. A. McCammon, J. Chem. Phys. **127**, 155101 (2007).
[28] H.-A. Yu and M. Karplus, J. Chem. Phys. **89**, 2366 (1988).
[29] D. Ben-Amotz, F. O. Raineri, and G. Stell, J. Phys. Chem. B **109**, 6866 (2005).
[30] M. Neumann, Mol. Phys. **57**, 97 (1986).
[31] D. V. Matyushov and B. M. Ladanyi, J. Chem. Phys. **110**, 994 (1999).
[32] D. Y. C. Chan, D. J. Mitchell, and B. W. Ninham, J. Chem. Phys. **70**, 2946 (1979).
[33] M. S. Wertheim, J. Chem. Phys. **55**, 4291 (1971).
[34] B. C. Freasier and D. J. Isbister, Mol. Phys. **38**, 81 (1979).
[35] B. Larsen, J. C. Rasaiah, and G. Stell, Mol. Phys. **33**, 987 (1977).
[36] S. Gupta and D. V. Matyushov, J. Phys. Chem. A **108**, 2087 (2004).
[37] D. V. Matyushov and B. M. Ladanyi, J. Chem. Phys. **107**, 5815 (1997).
[38] J. J. Weis, Mol. Phys. **100**, 579 (2002).
[39] S. Rajamani, T. Ghosh, and S. Garde, J. Chem. Phys. **120**, 4457 (2004).
[40] P. Frodl and S. Dietrich, Phys. Rev. A **45**, 7330 (1992).
[41] C.-Y. Lee, J. A. McCammon, and P. J. Rossky, J. Chem. Phys. **80**, 4448 (1984).
[42] F. H. Stillinger, J. Solution Chem. **2**, 141 (1973).
[43] P. K. Ghorai and D. V. Matyushov, J. Phys. Chem. A **110**, 8857 (2006).
[44] D. Ben-Amotz and R. Underwood, Acc. Chem. Res. **41**, 957 (2008).
[45] D. N. LeBard and D. V. Matyushov, J. Chem. Phys. **128**, 155106 (2008).
[46] A. Milischuk and D. V. Matyushov, J. Phys. Chem. A **106**, 2146 (2002).
[47] S. W. DeLeeuw, J. W. Perram, and E. R. Smith, Proc. R. Soc. London, Ser. A **373**, 27 (1980).
[48] G. Hummer, L. R. Pratt, and A. E. Garcia, J. Phys. Chem. A **102**, 7885 (1998).
[49] D. V. Matyushov, J. Chem. Phys. **122**, 044502 (2005).